UWB-Over-Fiber Communications: Modulation and Transmission

Shilong Pan, *Member, IEEE, OSA*, and Jianping Yao, *Senior Member, IEEE, Fellow, OSA*

(Invited Paper)

***Abstract*—The distribution of ultra-wideband (UWB) signals over optical fiber, or UWB over fiber (UWBoF), is proposed to extend the area of coverage and to offer the availability of undisrupted service across different networks. Various techniques have been reported recently for optical UWB pulse generation, but the study on the implementation of different modulation schemes based on these UWB pulses has just started. In addition, the influence of fiber dispersion on the power spectral density (PSD) of an UWB signal, and the bit-error-rate performance of an UWBoF system with different modulation schemes have not been systematically investigated. In this paper, we perform a comprehensive investigation of techniques to implement on–off keying (OOK), bi-phase modulation (BPM), pulse-amplitude modulation (PAM), pulse shape modulation (PSM), and pulse-position modulation (PPM) based on a phase modulator and an asymmetric Mach–Zehnder interferometer (AMZI). The AMZI is electrically reconfigurable by employing a polarization modulator (PolM). UWB signals with OOK, BPM, PAM, PSM, and PPM are realized by adjusting the polarization controllers in the AMZI and the amplitude of the electrical drive signal to the PolM. The UWB signals with OOK, BPM, PAM, and PSM are transmitted over a wired (single-mode fiber) and wireless link. Error-free operation is obtained for all the modulation schemes. The power penalties of transmission are less than 1.8 dB. The fiber dispersion on the PSD of the UWB signals is also theoretically studied and experimentally evaluated. An excellent agreement between the theoretical and the experimental results is achieved. The system is potentially integratable, which may provide a simple and cost-effective solution for UWBoF applications.**

***Index Terms*—Bi-phase modulation (BPM), microwave photonics, power spectral density (PSD), pulse-amplitude modulation (PAM), pulse-position modulation (PPM), pulse-shape modulation (PSM), ultra wideband (UWB), UWB over fiber.**

I. Introduction

THE future wireless personal-area networks require a low complexity, low cost, low power consumption, and high-data-rate wireless connectivity within the personal operating space. This network, however, is restricted by the reality of radio system engineering, where very limited free spectrum resources are available in the industrialized regions of the world. Under this background, ultra-wideband (UWB) radio technology, which optimally shares the existing radio spectrum resource rather than looking for new spectral bands, has been developed and become a topic of interest recently [1]–[5]. The key feature of an UWB system is the ability to spread a signal over a sufficiently wide bandwidth to ensure a low power spectral density (PSD) with negligible interferences with existing wireless systems. In 2002, the U.S. Federal Communications Commission (FCC) approved the unlicensed use of a spectral band from 3.1 to 10.6 GHz with a transmitted PSD of less than -41.3 dBm/MHz for indoor wireless communications. Due to the low PSD of the transmitted signal, there is a tradeoff between the achievable data rate and the communication distance. Higher data rate results in a shorter communication distance, while a lower data rate leads to a relatively longer communication distance. The typical communication distance of an UWB system is a few meters to tens of meters. Such short-range networks would operate mainly in stand-alone mode, with nearly nonexistent integration into the fixed wired and wireless wide-area infrastructures. To increase the area of coverage and to offer the availability of undisrupted service across different networks, a technique to distribute UWB signals over optical fiber, or UWB over fiber (UWBoF), has been proposed [5]. In an UWBoF system, optical UWB signals are generated in the central office and distributed to the access points via optical fibers [6]–[17].

One of the key advantages of an UWBoF system is that the UWB signals can be generated directly in the optical domain with no need for extra electrical to optical conversion. In addition, the generation of UWB signals in the optical domain provides other features such as light weight, small size, large tunability, and immunity to electromagnetic interference. In the past few years, various techniques for UWB pulse generation were reported [17]–[28]. For a practical UWBoF communication system, the information must be encoded, which is done by using different pulse modulation schemes. Until now, many modulation schemes have been demonstrated in the electrical domain, such as on–off keying (OOK), pulse-position modulation (PPM), bi-phase modulation (BPM, also known as pulse-polarity modulation), pulse-amplitude modulation (PAM), and pulse-shape modulation (PSM). For UWBoF communications, the modulation schemes can be implemented in the optical domain. To implement OOK, PSM, BPM, PAM, or PPM, the amplitude, position, polarity, or shape of the UWB pulses from an UWB pulse generator should be switchable at a high speed. In the literature, several optical OOK modulation schemes have

Manuscript received November 15, 2009; revised January 17, 2010; accepted February 15, 2010. Date of current version August 06, 2010. This work was supported by the Natural Sciences and Engineering Research Council of Canada.

The authors are with the Microwave Photonics Research Laboratory, School of Information Technology and Engineering, University of Ottawa, Ottawa, ON K1N 6N5, Canada (e-mail: jpyao@site.uOttawa.ca).

Color versions of one or more of the figures in this paper are available online at http://ieeexplore.ieee.org.

Digital Object Identifier 10.1109/JLT.2010.2043713

been reported [13], [17]. The major limitation of using OOK in an UWB communication system is the presence of multipath effect, in which echoes of the original pulses make it difficult to determine the absence of a pulse (i.e., "0"). In addition, OOK is a binary modulation method, which cannot be extended to an M-ary modulation. Therefore, it is of great interest to implement other modulation formats, such as BPM, PSM, PAM, and PPM in the optical domain.

On the other hand, an UWB signal in an UWBoF system must be distributed to a remote site via optical fiber. Due to the wide bandwidth and high data rate of an UWB signal, the performance of an UWBoF system would be affected by the chromatic dispersion (CD) of the optical fiber. It is well known that the transmission performance of an optical system is mainly determined by the optical spectral width and the frequency chirp of the optical signal in propagation. A narrower optical spectral width would make an optical signal be more tolerant to the fiber CD, while a chirped optical signal can be easily distorted due to the fiber CD. For instance, the optical spectral width of an UWB pulse generated by the spectral shaping and frequency-to-time mapping technique is in the order of several nanometers [17], [18], while the same UWB pulse produced based on phase modulation and phase-to-intensity conversion has an optical spectral width of less than 0.2 nm [19]–[21]. As a result, an UWBoF system based on the UWB pulses generated by the technique in [17], [18] can only support fiber transmission within a short distance, while that based on the technique in [19]–[21] can transmit in an optical fiber over 20 km [14]. Apparently, to have a better tolerance to fiber CD, an optical UWB signal with a narrower optical spectral width is desirable.

Ideally, a single-sideband (SSB) plus carrier (SSB+C) UWB signal is immune to the effect of CD. However, to generate an SSB+C UWB signal, a wideband electrical differentiator (to generate an UWB monocycle) and a wideband hybrid coupler are required [29], making the system complicated and costly. As an alternative, we have recently proposed and demonstrated several techniques to generate a quasi-SSB (QSSB) plus carrier (QSSB+C) optical UWB signal [16], [19], [22]. The QSSB+C optical UWB signal occupies an optical bandwidth that is much narrower than that of a conventional double-sideband (DSB) with carrier UWB signal. Since a narrower optical spectral width would make an optical signal be more tolerant to the fiber CD, the generated QSSB+C optical UWB signal is expected to have a better performance when transmitted over an optical fiber. Meanwhile, we have also reported several UWB generation schemes, which can be reconfigured for the generation of UWB signals with multiple modulation formats [22], [30], but the fiber transmission performance of the schemes has not been investigated.

In this paper, we perform a comprehensive investigation of the technique to implement different modulation schemes based on a phase modulator (PM) and an electrical reconfigurable asymmetric Mach–Zehnder interferometer (AMZI). A simple model is developed to study the implementation of OOK, BPM, PAM, PSM, and PPM schemes. The PSD spectra of the signals based on these modulation schemes with and without single-mode fiber (SMF) transmission are investigated by numerical simulations. The results show that the fiber CD has a positive impact on the OOK, BPM, PSM, and PPM signals, while a negative but small impact on the PAM signal. The numerical results are then verified by an experiment. The OOK, BPM, PAM, and PSM UWB signals are experimentally generated using the reconfigurable UWB signal generator. Then, the UWB signals are transmitted through a wired (SMF) and wireless link. For all the modulation schemes, the system can reach an error-free transmission and the power penalties of the transmission are less than 1.8 dB. The electrical spectral properties of the UWB signals with different modulation schemes without and with fiber transmission are also studied.

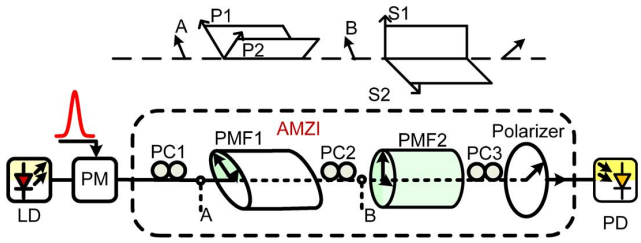

Fig. 1. Schematic of the optical UWB signal generator using a PM and a reconfigurable AMZI. LD: laser diode; PM: phase modulator; PC: polarization controller; PMF: polarization maintained fiber; PD: photodetector.

II. Principle

Fig. 1 shows the schematic of the reconfigurable UWB transmitter [19]. It consists of a laser diode (LD), a PM, an AMZI, and a photodetector (PD). A light wave from the LD is fiber coupled to the PM, which is driven by an electrical Gaussian pulse train. The phase-modulated optical signal is then sent to the AMZI. The AMZI consists of two sections of polarization maintaining fiber (PMF) followed by a polarizer. Three polarization controllers (PCs) are inserted to adjust the polarization states of light waves before PMF1, PMF2, and the polarizer. The PD is connected at the output of the polarizer to perform optical to electrical conversion.

A. UWB Pulse Generation

Mathematically, the normalized optical field at the output of the PM along the two polarization directions can be expressed as

$$e_{\mathrm{PM}}(t) = \begin{bmatrix} \exp[j\omega_c t + j\beta u(t)] \\ 0 \end{bmatrix} \tag{1}$$

where ω_c is the angular frequency of the optical carrier, β is the phase modulation index, and $u\,(t)$ is a normalized Gaussian pulse, which is given by

$$u(t) = \exp\left(-\frac{t^2}{2T_0^2}\right) \tag{2}$$

where T_0 is the half-width (at $1/e$-intensity point) of the Gaussian pulse.

The phase-modulated optical signal is then sent to the AMZI. The complex transfer matrix $T\,(\omega)$ of the PMF1 and PMF2 modules in the AMZI can be written as

$$T(\omega) = \begin{bmatrix} \cos\alpha_3 e^{j\phi_3} & -\sin\alpha_3 \\ \sin\alpha_3 & \cos\alpha_3 \end{bmatrix} \cdot \begin{bmatrix} e^{j\omega\tau_2} & 0 \\ 0 & 1 \end{bmatrix}$$

$$\cdot \begin{bmatrix} \cos\alpha_2 e^{j\phi_2} & -\sin\alpha_2 \\ \sin\alpha_2 & \cos\alpha_2 \end{bmatrix} \cdot \begin{bmatrix} e^{j\omega\tau_1} & 0 \\ 0 & 1 \end{bmatrix} \cdot \begin{bmatrix} \cos\alpha_1 e^{j\phi_1} & -\sin\alpha_1 \\ \sin\alpha_1 & \cos\alpha_1 \end{bmatrix} \tag{3}$$

where $\alpha_1, \alpha_2, \alpha_3$ are the rotation angles and ϕ_1, ϕ_2, ϕ_3 are the phase shifts introduced by PC1, PC2, and PC3, respectively. If the polarizer is adjusted to select the optical signal in $[\,1 \quad 0\,]'$ direction, we obtain the optical field at the output of the polarizer

$$\begin{aligned} E_{\mathrm{POL}}(\omega) &= [\,1 \quad 0\,] \cdot T(\omega) \cdot E_{\mathrm{PM}}(\omega) \\ &= \Big\{ \cos\alpha_3 \cos\alpha_2 \cos\alpha_1 e^{j[\omega(\tau_1+\tau_2)+\phi_1+\phi_2+\phi_3]} \\ &\quad - \sin\alpha_3 \sin\alpha_2 \cos\alpha_1 e^{j[\omega\tau_1+\phi_1]} \\ &\quad - \cos\alpha_3 \sin\alpha_2 \sin\alpha_1 e^{j[\omega\tau_2+\phi_3]} \\ &\quad - \sin\alpha_3 \cos\alpha_2 \sin\alpha_1 \Big\} \\ &\quad \cdot \tilde{F}\{\exp[j\omega_c t + j\beta u(t)]\} \end{aligned} \tag{4}$$

where $\tilde{F}\{\,\}$ denotes the Fourier transform. Converting (4) from the frequency domain to the time domain, we have

$$\begin{aligned} e_{\mathrm{POL}}(t) = -\exp(j\omega_c t) \Big\{ & \sin\alpha_3 \cos\alpha_2 \sin\alpha_1 e^{j\beta u(t)} \\ & + \sin\alpha_3 \sin\alpha_2 \cos\alpha_1 e^{j[\theta_1+\beta u(t+\tau_1)]} \\ & + \cos\alpha_3 \sin\alpha_2 \sin\alpha_1 e^{j[\theta_3+\beta u(t+\tau_2)]} \\ & - \cos\alpha_3 \cos\alpha_2 \cos\alpha_1 \\ & \times e^{j[\theta_1+\phi_2+\theta_3+\beta u(t+\tau_1+\tau_2)]} \Big\} \end{aligned} \tag{5}$$

where $\theta_1 = \omega_c\tau_1 + \phi_1$ and $\theta_3 = \omega_c\tau_2 + \phi_3$. In our configuration, α_2 and α_3 are fixed at $\pi/4$, so (5) can be simplified to

$$\begin{aligned} e_{\mathrm{POL}}(t) = -\frac{1}{2}\exp(j\omega_c t) \Big\{ & \sin\alpha_1 e^{j\beta u(t)} \\ & + \cos\alpha_1 e^{j[\theta_1+\beta u(t+\tau_1)]} \\ & + \sin\alpha_1 e^{j[\theta_3+\beta u(t+\tau_2)]} \\ & - \cos\alpha_1 e^{j[\theta_1+\phi_2+\theta_3+\beta u(t+\tau_1+\tau_2)]} \Big\}. \end{aligned} \tag{6}$$

If the optical signal expressed in (6) is sent to a PD for square-law detection, the ac term of the photocurrent is

$$\begin{aligned} i(t) \propto & \sin 2\alpha_1 \cos[\beta u(t+\tau_1) - \beta u(t) + \theta_1] \\ & + (1 - \cos 2\alpha_1) \cos[\beta u(t+\tau_2) - \beta u(t) + \theta_3] \\ & - \sin 2\alpha_1 \cos[\beta u(t+\tau_1+\tau_2) \\ & - \beta u(t) + \theta_1 + \phi_2 + \theta_3] \\ & + \sin 2\alpha_1 \cos[\beta u(t+\tau_2) \\ & - \beta u(t+\tau_1) + \theta_3 - \theta_1] \\ & - (1 + \cos 2\alpha_1) \cos[\beta u(t+\tau_1+\tau_2) \\ & - \beta u(t+\tau_1) + \phi_2 + \theta_3 \\ & - \sin 2\alpha_1 \cos[\beta u(t+\tau_1+\tau_2) \\ & - \beta u(t+\tau_2) + \phi_2 + \theta_1]. \end{aligned} \tag{7}$$

To generate an UWB Gaussian monocycle, we should align the polarization direction of the modulated light wave with one principal axis of PMF1 (i.e., $\alpha_1 = 0$ or $\pi/2$) and let $\phi_2 = 0$, and $\theta_3 = \pi/2$. Equation (7) is simplified to

$$i(t) \propto \begin{cases} \sin\beta[u(t+\tau_1+\tau_2) - u(t+\tau_1)] & \alpha = 0 \\ -\sin\beta\,[u\,(t+\tau_2) - u(t)] & \alpha = \pi/2. \end{cases} \tag{8}$$

For small-signal modulation, β is very small, we have $\sin[\beta u(t)] \approx \beta u(t)$, then (8) is approximated

$$i(t) \propto \begin{cases} \beta[u(t+\tau_1+\tau_2) - u(t+\tau_1)] & \alpha = 0 \\ -\beta[u(t+\tau_2) - u(t)] & \alpha = \pi/2. \end{cases} \tag{9}$$

As can be seen, the output current is proportional to the first-order difference of the input Gaussian signal. If τ_1 is sufficiently small, the first-order difference can be approximated as the first-order derivative; therefore, the entire system is equivalent to a first-order differentiator and a Gaussian monocycle is generated [5]. By simply alternating α_1 from 0 to $\pi/2$ via tuning PC1, the polarity of the generated monocycle will be inverted. It should be noted that the monocycle pulses with opposite polarities would have a time shift of τ_1, which is not desirable for some modulation schemes, such as BPM. One possible solution is to change θ_3 or ϕ_2 instead of changing α_1. For instance, fix α_1 at $\pi/2$ and let $\theta_3 = \pm\pi/2$, (7) is approximately given

$$i(t) \propto \pm\beta[u(t+\tau_2) - u(t)]. \tag{10}$$

In this case, the UWB monocycles with opposite polarities will not have a time shift.

On the other hand, when the polarization direction of the modulated light wave is oriented to have an angle of 45° to one principal axis of PMF1 (i.e., $\alpha_1 = \pm\pi/4$), and let $\theta_1 = \pi/2, \phi_2 = 0$, and $\theta_3 = \pm\pi/2$, we have

$$\begin{aligned} i(t) \propto \pm\{ & -\sin[\beta u(t+\tau_1) - \beta u(t)] \\ & - \sin[\beta u(t+\tau_2) - \beta u(t)] \\ & + \cos[\beta u(t+\tau_1+\tau_2) - \beta u(t)] \\ & + \cos[\beta u(t+\tau_2) - \beta u(t+\tau_1)] \\ & + \sin[\beta u(t+\tau_1+\tau_2) - \beta u(t+\tau_1)] \\ & + \sin[\beta u(t+\tau_1+\tau_2) - \beta u(t+\tau_2)]\}. \end{aligned} \tag{11}$$

Again, if small-signal modulation is assumed, the six terms on the right-hand side of (11) can be expanded in Taylor series. By neglecting the second- and higher order terms, (11) is simplified to

$$\begin{aligned} i(t) \propto \pm 2\beta[& u(t+\tau_1+\tau_2) \\ & - u(t+\tau_2) - u(t+\tau_1) + u(t)]. \end{aligned} \tag{12}$$

As can be seen, the current is proportional to the second-order difference of the input Gaussian signal. If τ_1 and τ_2 are sufficiently small, the second-order difference can be approximated as the second-order derivative; therefore, the entire system is

equivalent to a second-order differentiator and a Gaussian doublet is generated. The ± sign in (12) corresponds to the two opposite polarities.

Substituting $\theta_3 = \pi/2, \phi_2 = 0$, and $\alpha_1 = 0$ or $\pi/2$ back to (6) and employing the small-signal modulation assumption, we can obtain the optical field $e_{\mathrm{M}\pm}(t)$ as

$$e_{\mathrm{M}+}(t) = -\frac{1}{2}\exp(j\omega_c t + j\theta_1) \times \{(1-j)+j\beta[u(t+\tau_1)-ju(t+\tau_1+\tau_2)]\} \quad (13a)$$

$$e_{\mathrm{M}-}(t) = -\frac{1}{2}\exp(j\omega_c t) \times \{(1+j)+j\beta[u(t)+ju(t+\tau_2)]\}. \quad (13b)$$

From (13), we can see the phase term of the generated UWB Gaussian monocycle is a function of time; therefore, the pulses are chirped. Converting (13) from the time domain to the frequency domain, we have

$$E_{\mathrm{M}+}(\omega) = -\frac{1}{2}\exp(j\theta_1) \times \left\{2\pi(1-j)\delta(\omega-\omega_c) + j\beta e^{j(\omega-\omega_c)\tau_1} \times \left[1 - je^{j(\omega-\omega_c)\tau_2}\right]U(\omega-\omega_c)\right\} \quad (14a)$$

$$E_{\mathrm{M}-}(\omega) = -\frac{1}{2}\left\{2\pi(1+j)\delta(\omega-\omega_c) + j\beta\left[1+je^{j(\omega-\omega_c)\tau_2}\right]U(\omega-\omega_c)\right\} \quad (14b)$$

where $U(\omega) = \tilde{F}\{u(t)\}$ is the Fourier transform of the input Gaussian pulse. Accordingly, the optical power spectrum of the generated optical Gaussian monocycle can be written as

$$P_{\mathrm{M}\pm}(\omega) = |\tilde{F}\{e_{\mathrm{M}\pm}(t)\}|^2 = 2\pi^2\delta(\omega-\omega_c) + \frac{1}{2}\beta^2[1 \pm \sin(\omega-\omega_c)\tau_2]U^2(\omega-\omega_c). \quad (15)$$

From (15), the optical power spectrum is asymmetric, which consists of an optical carrier and a Gaussian lobe filtered by a system having a sine-based asymmetry transfer function. The profile would be similar to the optical spectrum of an SSB+C signal. The pulse was named as a QSSB-UWB monocycle in [31].

Using a similar mathematical manipulation, we can express the optical field $e_{\mathrm{D}\pm}(t)$, optical field spectrum $E_{\mathrm{D}\pm}(\omega)$, and optical power spectrum $P_{\mathrm{D}\pm}(\omega)$ of the Gaussian doublets as

$$e_{\mathrm{D}\pm}(t) = -\frac{\sqrt{2}}{4}\exp(j\omega_c t) \times \{2(\pm 1+j)+\beta[\pm ju(t)\pm ju(t+\tau_1+\tau_2) - u(t+\tau_1)-u(t+\tau_2)]\} \quad (16)$$

$$E_{\mathrm{D}\pm}(\omega) = -\frac{\sqrt{2}}{4}\left\{4\pi(\pm 1+j)\delta(\omega-\omega_c) + \beta\left[\pm j - e^{j(\omega-\omega_c)\tau_1} - e^{j(\omega-\omega_c)\tau_2} \pm je^{j(\omega-\omega_c)(\tau_1+\tau_2)}\right]U(\omega-\omega_c)\right\} \quad (17)$$

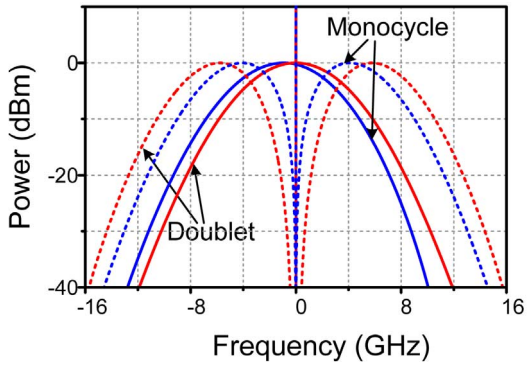

Fig. 2. Simulated optical spectra of the proposed UWB monocycle and doublet pulses (solid line), and the DSB UWB monocycle and doublet pulses (dashed line).

$$P_{\mathrm{D}\pm}(\omega) = 4\pi^2\delta(\omega-\omega_c) + \frac{1}{2}\beta^2[1+\cos(\omega-\omega_c)\tau_1 \cos(\omega-\omega_c)\tau_2]U^2(\omega-\omega_c). \quad (18)$$

Again, the generated UWB Gaussian doublet pulses are chirped. But the optical power spectrum is symmetric, and the 3-dB bandwidth is narrower than that of a Gaussian pulse.

Fig. 2 illustrates the simulated optical power spectra of the generated UWB monocycle and doublet pulses (solid line). As a comparison, the optical power spectra of a DSB UWB monocycle and a doublet pulse obtained by directly sending an electrical Gaussian monocycle or doublet to a MZM are also shown (dashed line). In the simulations, the time-domain waveforms of the generated UWB pulses and the DSB UWB pulses are set to be the same. The 3-dB bandwidths for the QSSB and DSB UWB monocycles are 6.40 and 13.34 GHz, and the 10-dB bandwidths are 11.65 and 18.04 GHz, respectively. The 3-dB bandwidths of the proposed UWB doublet and the DSB UWB doublet are 6.41 and 16.62 GHz, and the 10-dB bandwidths are 11.68 and 21.12 GHz, respectively. Apparently, the proposed UWB pulses have an optical bandwidth much narrower than that of the DSB UWB pulses. In addition, the proposed UWB Gaussian monocycle and doublet pulses occupy almost the same optical spectral bandwidth. Because the optical spectral widths of the generated UWB pulses are very narrow, they should have a good tolerance to fiber CD although the pulses are chirped.

B. Implementation of the Modulation Schemes

Since the proposed scheme in Fig. 1 can generate UWB Gaussian monocycle and doublet pulses with opposite polarities by adjusting the PCs in the AMZI, different modulation scheme can be performed if the PCs are replaced by high-speed polarization modulators (PolMs). A PolM is a special PM that can support both TE and TM modes with however opposite phase modulation indexes [32]. When a linearly polarized incident light oriented at an angle of 45° to one principal axis of the PolM is sent to the input of the PolM, the signal is projected equally to the two principal axes and will experience complementary phase modulations if an electrical drive signal is applied to the PolM via the RF port. Since the phase modulations can be converted to polarization rotation by a PC, the PolM can switch the optical light wave between two arbitrary

polarization states when two PCs are incorporated at the input and output of the PolM, with the first PC being used to adjust the polarization direction of the incident light wave to have an angle of 45° with respect to one principal axis of the PolM, and the second PC being used to obtain two desired output polarization states.

As indicated in the previous subsection, when the polarization direction of the light wave at point A in Fig. 1 is aligned with one principal axis of PMF1 (e.g., P1), an UWB monocycle would be generated at the output of the PD. If the light wave at point A is aligned with the other principal axis of PMF1 (e.g., P2), the polarity of the generated monocycle pulse would be inverted. Therefore, by inserting a PolM before PMF1 to switch the polarization direction of the light wave at point A between P1 and P2, a bi-phase-modulated UWB monocycle signal is generated.

To implement BPM of UWB doublet pulses, two parameters α_1 and θ_3 should be changed simultaneously, which requires the use of two PolMs that are placed before PMF1 and after PMF2. This approach is complicated and costly. To implement BPM of UWB doublet pulses using a single PolM, we can configure the system by letting $\phi_2 = \pi, \theta_1 = \pi, \theta_3 = -\pi/2$, and $\alpha_1 = \pi/4 \pm \sigma$, where σ is much smaller than $\pi/4$. If small-signal modulation is assumed, (7) is simplified to

$$i(t) \propto \mp 2\sigma\beta[u(t+\tau_1+\tau_2) - u(t+\tau_2) - u(t+\tau_1) + u(t)]. \quad (19)$$

Equation (19) is the expression for an UWB Gaussian doublet, where the $\pm$ sign represents the two opposite polarities. If the PolM switches α_1 between $\pi/4 - \sigma$ and $\pi/4 + \sigma$, BPM of the UWB doublet pulses is achieved.

The PSM can be realized by using a monocycle pulse to represent a 0 bit and a doublet pulse to represent a 1 bit or vice versa, which can be implemented by using the PolM to align the polarization direction of the light wave at point A with P1 or to have an angle of 45° with respect to P1.

To implement PAM, the system should have different transmittance for the 0 and 1 bits. This can be accomplished by adjusting the polarization state of the light wave at point A. For example, Fig. 3 shows two Gaussian monocycle pulses obtained when $\alpha_1 = 0$ and $\alpha_1 = 0.05\pi$. The two pulses have different amplitudes that can be used to implement PAM by letting the two pulses to represent the 1 and 0 bits. It should be noted that the low amplitude of the monocycle pulse also means only a small portion of the phase modulation being converted to intensity variations. Large phase variation is still maintained, so the chirp of the pulse generated when $\alpha_1 = 0.05\pi$ would be remarkable.

For OOK, there should be no intensity variation for the 0 bits, which can be accomplished by aligning the polarization state of the incident light wave to one of the principal states of polarization (PSPs) [33]. Assuming $\phi_2 = 0$ and $\theta_3 = \pi/2$, the Jones vector of the PSPs of the PMF1 and PMF2 module can be written as [33]

$$\hat{\varepsilon}_{\pm} = \frac{\sqrt{2}}{2} e^{j\rho} \begin{bmatrix} \frac{[k_{\pm} - (\tau_2 - \tau_1)]e^{-\frac{j}{2}\omega\tau_1}}{D_{\pm}} \\ -j\frac{[(\tau_1 + \tau_2) - k_{\pm}]e^{\frac{j}{2}\omega\tau_1}}{D_{\pm}} \end{bmatrix} \quad (20)$$

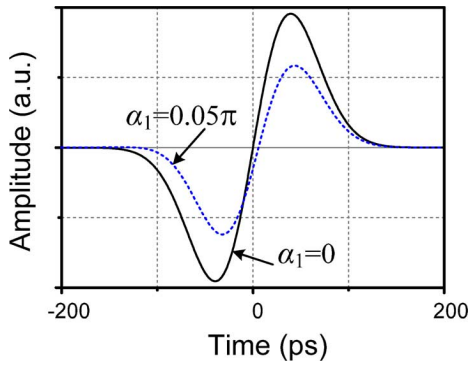

Fig. 3. Optical UWB monocycle pulses obtained when $\alpha_1 = 0$ (solid line), and $\alpha_1 = 0.05\pi$ (dashed line). Other parameters: $\theta_1 = \pi, \phi_2 = 0$, and $\theta_3 = \pi/2$.

where ρ is an arbitrary phase and

$$k_{\pm} = \pm\sqrt{\tau_1^2 + \tau_2^2} \quad (21)$$

$$D_{\pm} = \sqrt{2k_{\pm}(k_{\pm} - \tau_2)}. \quad (22)$$

If τ_1 is sufficiently small, the PSPs can be considered to be wavelength independent. In that way, phase modulation will not be converted into intensity modulation when the incident light wave is aligned with one of the PSPs. Then, if the light wave at point A is aligned with one of the PSPs when the PolM is driven by 0 bits, and aligned with P1 when the PolM is driven by 1 bits, OOK modulation is realized.

The transmitter can also be reconfigured to obtain PPM by placing the PolM between PMF1 and PMF2. The PM and PMF1 are employed to generate UWB monocycle, and PMF2 is used as a time-delay module. The polarization direction of the light wave at point B is aligned with the fast axis of PMF2, when the PolM is driven by 1 bits, and otherwise it is aligned with the slow axis of PMF2 when the PolM is driven by 0 bits. As a result, the position of the pulses is changed according to the marks or spaces in the data signal. PPM is thus implemented.

C. PSD Analysis of the UWB Signals in Propagation

Because UWB signals should coexist with other narrowband wireless systems operating in the same frequency band with negligible mutual interferences, the PSD of an UWB signal is very important for the design and deployment of a practical UWB system. It is known that UWB signals with different modulation schemes would have different PSD. In this section, the PSD of UWB signals with different modulation schemes with and without optical fiber transmission will be investigated.

Generally, a data-modulated UWB signal can be represented by

$$x(t) = \sum_{n=-\infty}^{\infty} [(1 - a_n) f_0(t - nT - \mu_n) + a_n f_1(t - nT - \mu_n)] \quad (23)$$

where $\{a_n\}$ is a binary independent and identically distributed (i.i.d.) random sequence with a probability density function P

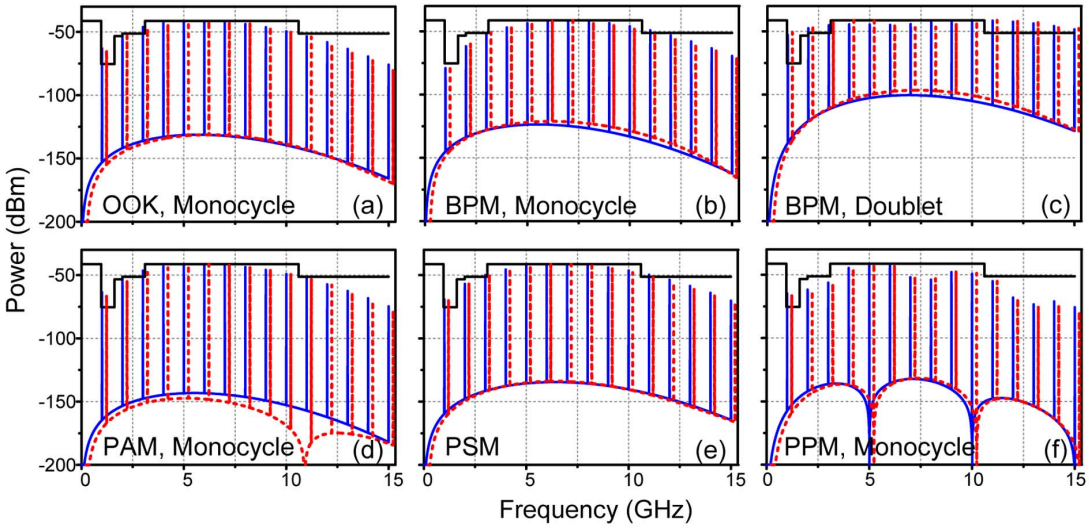

Fig. 4. PSD spectra of the radiated UWB signals with OOK, BPM, PAM, PSM, and PPM schemes. Solid lines: back to back; dashed line: with 20-km SMF transmission. $\tau_1 = 20$ ps, $T = 1$ ns, $p = 0.5$, and $\Delta = 0$. For OOK, BPM, PAM, PSM: $\tau_2 = 20$ ps; for PPM: $\tau_2 = 200$ ps.

$(a_n = 1) = p, T$ is the bit period, f_0 and f_1 are the waveforms representing bits "0" and "1," respectively, and μ_n is the time hopping time shift [4], which is uniformly distributed in $[-\Delta, \Delta]$. From [31], the PSD for the radiated signal $x(t)$ is expressed as

$$S_R(\omega) \propto \omega^2 S(\omega) = \omega^2 S_C(\omega) + \omega^2 S_D(\omega) \tag{24}$$

where $S_C(\omega)$ and $S_D(\omega)$ denote the continuous part and the discrete part of the PSD, respectively, which are given by

$$\begin{aligned} S_C(\omega) = {} & \frac{|F_0(\omega)|^2}{T}\left[(1-p) - (1-p)^2 \sin c^2\left(\frac{\omega\Delta}{2}\right)\right] \\ & + \frac{|F_1(\omega)|^2}{T}\left[p - p^2 \sin c^2\left(\frac{\omega\Delta}{2}\right)\right] \\ & - \frac{[F_0(\omega)F_1^*(\omega) + F_0^*(\omega)F_1(\omega)]}{T} \\ & \times p(1-p)\sin c^2\left(\frac{\omega\Delta}{2}\right) \end{aligned} \tag{25a}$$

$$\begin{aligned} S_D(\omega) = {} & \frac{1}{T^2}\sum_{n=-\infty}^{\infty}\delta\left(\omega - \frac{2\pi n}{T}\right) \\ & \times \left[|F_0(\omega)|^2(1-p)^2 \sin c^2\left(\frac{\omega\Delta}{2}\right)\right. \\ & + |F_1(\omega)|^2 p^2 \sin c^2\left(\frac{\omega\Delta}{2}\right) \\ & + [F_0(\omega)F_1^*(\omega) + F_0^*(\omega)F_1(\omega)] \\ & \left. \times p(1-p)\sin c^2\left(\frac{\omega\Delta}{2}\right)\right] \end{aligned} \tag{25b}$$

where $F_0(\omega)$ and $F_1(\omega)$ are the Fourier transforms of f_0 and f_1, respectively. From (24) and (25), the PSD of a radiated UWB signal is determined by five parameters, i.e., $F_0(\omega), F_1(\omega), T, p$, and Δ. Since T, p, and Δ are time invariant in transmission, and $F_0(\omega)$ and $F_1(\omega)$ can be obtained by (9) and (12), the PSD can be numerically calculated. To include the transmission effects in the optical fiber, the split-step Fourier method can be employed to solve the nonlinear Schrödinger equation [34], to numerically calculate the optical field of the UWB signal in propagation. $F_0(\omega)$ and $F_1(\omega)$ can then be obtained by performing Fourier transformation of the optical field.

Fig. 4(a) shows the PSD spectra of a radiated OOK UWB monocycle signal without fiber transmission and with 20-km SMF transmission. To avoid overlap, in Fig. 4, the PSD spectrum of the UWB signal with 20-km SMF transmission is manually shifted by ~0.15 GHz. The PSD spectrum consists of continuous and discrete components. Theoretically, the ratio of the powers between the discrete lines and the continuous parts are $p/T\ (1-p)$. For $p = 0.5$ and $T = 1$ ns, this ratio is as large as 10^9 [31]. As expected, in Fig. 4(a) the discrete lines are 90 dB higher over their continuous counterparts. The FCC-specified indoor spectral mask is also plotted for comparison. The spectral peaks of the UWB signals are controlled to be -41.3 dBm. As can be seen, the UWB monocycle exceeds the FCC mask in the spectral range from 0.96 to 3.1 GHz. In a practical UWBoF system, the UWB antennas would have a lower gain in the low-frequency region, so the spectral lines in the low-frequency range would be suppressed. Because the powers of these low-frequency spectral lines are more than 5 dB lower than that of the spectral peak, the suppression of them does not cause significant power loss. After 20-km SMF transmission, the components in the 3.1–10.6 GHz band are enhanced since the residual phase variation (chirp) in the pulse is converted into intensity variation by the fiber CD, which would increase the total transmitted power. On the other hand, the spectral lines with a frequency larger than 11 GHz are suppressed due to the low-pass equivalent transfer function of the dispersive medium [35]. As a result, the undesirable spectral lines in the range from 0.96 to 3.1 GHz and with a frequency larger than 10.6 GHz are reduced by more than 1 dB. Therefore, we can conclude that the fiber CD has a positive impact on the OOK-modulated UWB signal.

Fig. 4(b) shows the PSD spectra of a radiated BPM UWB monocycle signal. Ideally, if $p = 0.5$ and $f_0 = -f_1$, the discrete part of the PSD of a BPM signal should equal to 0. In a practical system, however, it is very hard to keep exactly $p = 0.5$ and $f_0 = -f_1$. If p slightly deviates from 0.5, or f_0 does not equal to

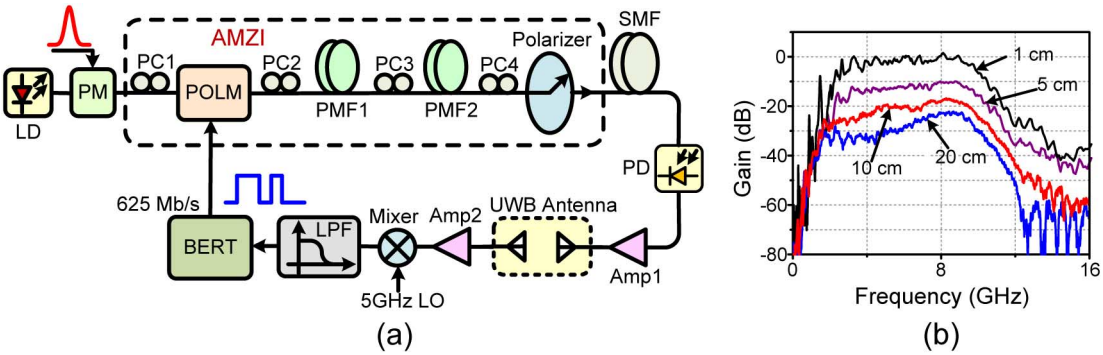

Fig. 5. (a) Experimental setup of the UWBoF system reconfigurable for multiple modulation formats (b) Frequency response of the UWB antennas pair placed in their peak radiation direction in the azimuth plane with a distance of 1, 5, 10, and 20 cm. PolM: polarization modulator; SMF: single-mode fiber; Amp: electrical amplifier; LO: local oscillator; LPF: low-pass filter; BERT: bit error rate tester.

$-f_1$, strong discrete lines would be present in the PSD spectra. From (9), there is a time shift for the UWB monocycles with opposite polarities, so the discrete components are maintained in the PSD spectra. In a frequency range from 1 to 11 GHz, the power differences of the discrete lines and their continuous counterparts increase from 65 to 88 dB, which make the PSD of the BPM UWB signal fit the FCC mask very well. Meanwhile, the power of the continuous part is much greater than that of an OOK UWB signal. Since the data information is included in the continuous part, the system employing BPM should have a higher receiver sensitivity than that using OOK. After 20-km SMF transmission, the power difference between the discrete lines and their continuous counterparts in the frequency range of 3–14 GHz is reduced because the transmission introduces new time shift for the UWB monocycles with opposite polarities [31]. This time shift would partly cancel out the time shift of the original pulses. Thus, we can conclude again that the fiber CD has a positive impact on the BPM-UWB signals. For the BPM UWB doublet signal, as shown in Fig. 4(c) and (h), the discrete lines in the range from 3 to 11 GHz are only 56 to 66 dB higher over the continuous part because the time shift between the UWB doublets with opposite polarities is almost equals to 0. In addition, the 20-km SMF transmission reduces the discrete lines by 4–8 dB, which is desirable for the UWBoF system.

The PAM is usually used in duo-binary systems. Compared with other modulation schemes, the modulation efficiency is relatively low. As can be seen from their PSD spectra, as shown in Fig. 4(d), the discrete lines are 101-dB higher than their continuous counterparts. After 20-km SMF transmission, the discrete lines in the 3.1–10.6 GHz band are enhanced, while the continuous part is further reduced. Because both the pulses to represent 0 and 1 bits are chirped, in the SMF, the fiber CD would convert the phase variation to intensity variation. The amplitude of the pulses to represent 0 bits would be increased more since the chirp in the pulses is larger than that in the pulses to represent 1 bits. As a result, the amplitude difference between the pulses representing 0 and 1 bits becomes smaller, which further decreases the modulation efficiency. Thus, the fiber CD would deteriorate the performance of the PAM-based UWBoF system.

Fig. 4(e) shows the PSD spectra of the radiated PSM UWB signals in which a monocycle pulse is employed to represent a 0 bit and a doublet pulse is employed to represent a 1 bit. The power of the discrete lines are more than 90-dB higher over their continuous counterparts. Since the signal consists of monocycle and doublet pulses, the PSD spectra fit the FCC mask well except for the spectral line at 1 GHz, which has a power density that exceeds the FCC mask by 6 dB. By fiber transmission, the frequency components from 5–7 GHz are enhanced because the chirp in the UWB pulses is converted into intensity variation. Meanwhile, the difference between the discrete and continuous parts is decreased by $\sim$1 dB. Again, the fiber CD has a positive impact on the PSM-UWB signals.

For PPM, both the discrete and the continuous parts of the PSD are the power spectrum of an UWB pulse multiplied by a cosine-based function, which is periodic in frequency [31]. The period is $1/T_{\rm b}$, where $T_{\rm b}$ is the time shift of the pulses for 0 and 1 bits. In the calculation, we set $T_b = 200$ ps, so the period is 5 GHz. Fig. 4(f) shows the PSD of a radiated PPM UWB monocycle signal. The transmission performance is almost identical to that of an OOK UWB signal. The spectral components in the 3.1–10.6 GHz band are enhanced, while those in other bands are reduced, so the fiber CD also contributes positively to the PPM-UWB signals.

III. Experiment Setup

An experiment is performed based on the experimental setup, as shown in Fig. 5(a). A light wave from the LD (Yokogawa AQ2201) is sent to a $LiNbO_3$ PM. A pulse train generated by a bit-error-rate tester (BERT) (Agilent 4901B) with a fixed pattern "1000 0000 0000 0000" (one "1" every 16 bits) and a bit rate of 10 Gb/s, which is equivalent to a pulse train with a repetition rate of 625 MHz and a duty cycle of about 1/16, is applied to the PM to phase modulate the light wave. The input pulse has a shape close to a Gaussian with a full-width at half-maximum of about 85 ps. The AMZI consists of a PolM (Versawave Technologies), two sections of PMF (Corning PM1550, 29.1 and 14.6 m), four PCs, and a polarizer. The differential group delays (DGDs) of the two PMF sections are about 20.1 and 40.1 ps. A 625-Mb/s data signal with a fixed pattern "01101001" or a $2^{31}-1$ pseudo-random binary sequence (PRBS) generated by a second BERT (Anritsu ME522A) is used to drive the PolM.

To evaluate the transmission performance, the generated UWB signal is distributed over an SMF link and then detected by a PD. The obtained electrical signal is emitted to free space through a commercially available UWB omni-directional antenna (Skycross SMT-3TO10M-A). At the UWB receiver, the

radiated UWB signal is received by another UWB antenna, and amplified by a wideband electrical amplifier (EA, 25-dB gain). The frequency responses of the antennas pair with a distance of 1, 5, 10, and 20 cm are shown in Fig. 5(b). As can be seen, a larger distance results in a higher insertion loss. Due to the limited gain provided by the EA, in our experiment the antennas are placed in their peak radiation direction in the azimuth plane with a distance of 10 cm. The 10-dB bandwidth of the antennas pair is about 8.1 GHz (2.5–10.6 GHz). The signal from the amplifier is mixed at an electrical mixer with a local oscillator (LO) signal at 5 GHz followed by a low-pass filter (LPF, 3-dB bandwidth of 470 MHz), to down-convert the data signal from a center frequency of about 5 GHz to the baseband. At the output of the LPF, the received baseband signal is introduced to the BERT for bit-error-rate (BER) measurement. The waveforms are observed by a high-speed sampling oscilloscope (Agilent 86116A), and the spectra are measured by an electrical spectrum analyzer (ESA, Agilent E4448A).

IV. Results and Discussion

To verify the implementation of the different modulation schemes, a fixed code pattern "01101001" is used to drive the PolM. Fig. 6 shows the temporal waveforms of the optical UWB signals with OOK, BPM, PAM, and PSM. Excellent OOK, BPM, PAM, and PSM are realized by adjusting the PCs and the amplitude of the electrical drive signal to the PolM. Some undesirable parasitic pulses are also observed, which are produced by the transient state between "0" and "1" or "1" and "0" in the data signal. The presence of the parasitic pulses would add some low frequency components to the UWB signals and would deteriorate the performance of the UWB transmission system. Methods to eliminate the parasitic pulses are under investigation.

The electrical spectra of the UWB signals with different modulation schemes are shown in Fig. 7. The measurement is performed when the PolM is driven by a PRBS with a word length of $2^{31}-1$. As can be seen, all the spectra consist of continuous and discrete components. The discrete spectral lines are generally $\sim$20-dB higher than the continuous part, which is much less than the theoretically predicted value of $\sim$88 dB. This is because the resolution bandwidth of the ESA is 1 MHz, which is too low to make a precise measurement. The BPM-UWB signals have the largest continuous part, while the PAM-UWB signals have the largest discrete spectral lines, which agree with the simulations very well.

Fig. 8 shows the electrical spectra of the UWB signals in the UWBoF system with wireless and SMF transmission. The spectral peaks of these UWB signals are manually attenuated to be -41.3 dBm.

For the OOK signals, the fiber transmission enhances the discrete spectral lines in the 3.1–10.6 GHz band, because the residual phase modulation in the UWB pulses is converted into intensity variation. However, the continuous part is reduced. Although the 0 bits of the OOK UWB signal do not have intensity variations, they carry phase modulations. The phase modulation would be converted into intensity variation, which shapes the OOK signal to be similar to a PAM signal. As a result, the discrete lines are enhanced, while the continuous part is reduced.

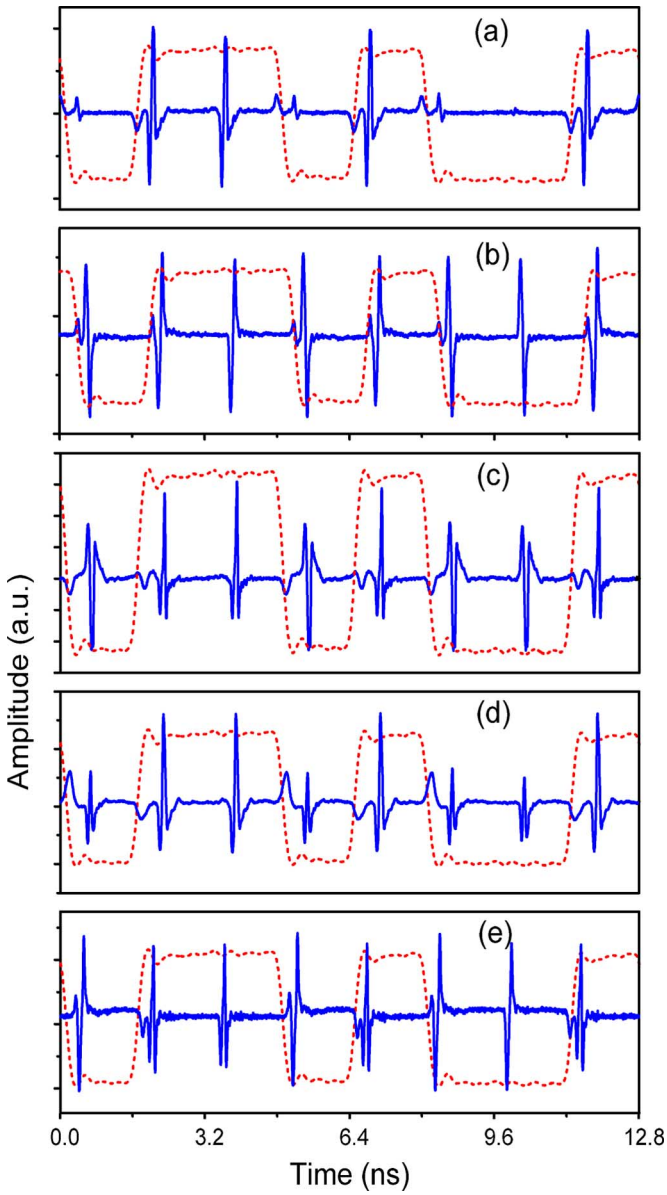

Fig. 6. Waveforms of the UWB signals with (a) OOK, (b), (c) BPM, (d) PAM, and (e) PSM.

In addition, the spectral line at 1.25 GHz is increased by 12 dB because the parasitic pulses are also enhanced by the fiber CD.

For the BPM signals, the continuous part in the frequency band of 3.1–10.6 GHz is significantly increased by the fiber CD since the fiber transmission reduces the time shift of the UWB monocycle pulses with opposite polarities. The discrete spectral lines of the PAM UWB signals are obviously enhanced, which equivalently decreases the power of the continuous part. Since the data information is mainly contained in the continuous part, the fiber CD would reduce the receiver sensitivity of a PAM-based UWBoF system. For the PSM signal, as predicted, the power of the continuous part is increased by fiber transmission.

It is worth noting that the BPM UWB signal in the aforementioned study is based on monocycle pulses and has a good transmission performance. However, the transmission performance of a BPM UWB doublet signal is poorer. Because of the small σ and β, as can be seen from (19), the amplitudes of the UWB

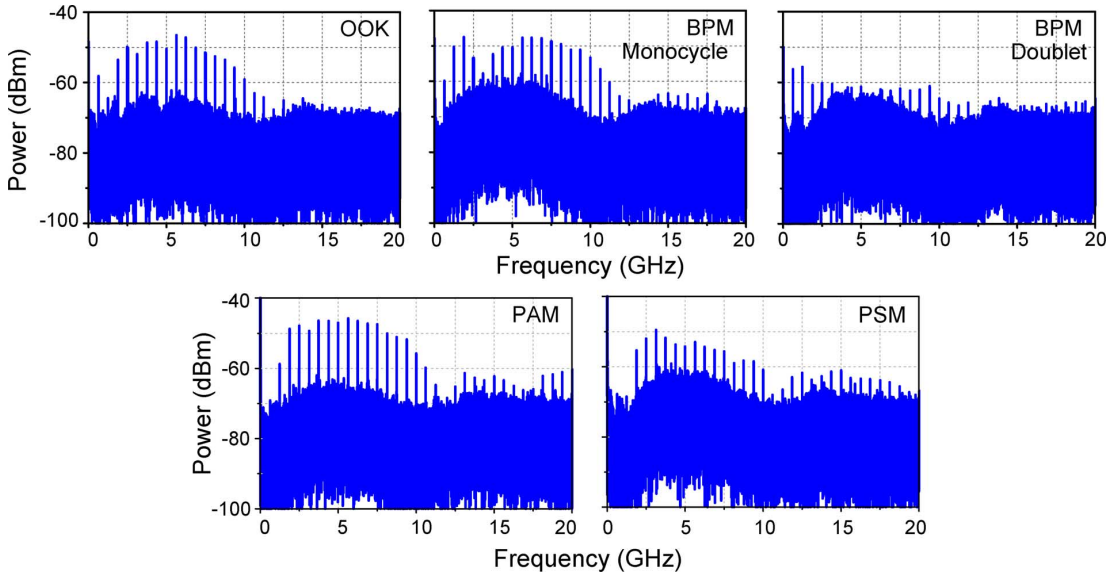

Fig. 7. Electrical spectra of the UWB signals with OOK, BPM, PAM, and PSM. $\mathrm{RBW} = 1$ MHz.

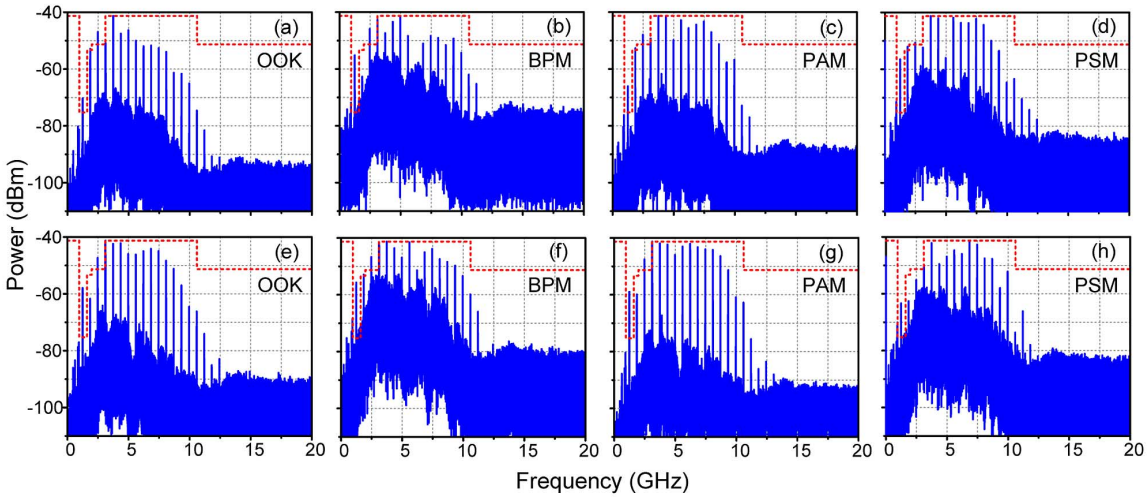

Fig. 8. Electrical spectra of the UWB signals with OOK, BPM, PAM, and PSM schemes (a)–(d) with wireless transmission; (f)–(j) with 20-km SMF and wireless transmission.

doublet pulses are very small, which would be significantly degraded by the amplified spontaneous emission noise from the erbium-doped fiber amplifiers. In addition, most of the phase variations due to phase modulation is kept in the UWB based on doublet pulses, so they can be easily distorted due to the fiber CD.

By down converting the data signal from a center frequency of 5 GHz to baseband, we can evaluate the BER performance of the UWBoF system with different modulation schemes [14]. Fig. 9 shows the BER measurements of the UWBoF system with OOK, BPM, PAM, and PSM. As expected, an UWB signal with PAM scheme has the poorest BER performance since the power of the continuous part is very small. The fiber transmission causes a 1.78-dB power penalty at 1×10^{-7}, which is also the largest among the four modulation schemes. On the other hand, an UWB signal with BPM scheme experiences a negative power penalty after 20-km SMF transmission because the power of its continuous part is enhanced by the fiber CD. Since the power of the continuous part of the PSM UWB signal is enhanced by fiber transmission, it should have a negative power penalty as well. However, the fiber CD also increases the amplitude of the undesirable parasitic pulses. As a result, a small power penalty of 0.34 dB is introduced by the fiber transmission. For the OOK signal, because the fiber CD would shape it to a PAM signal, the power penalty is larger (0.51 dB). Nevertheless, for all the modulation schemes, the system can reach an error-free operation with an acceptable low power penalty ($<$1.8 dB).

When the PolM is placed between PMF1 and PMF2, PPM can be implemented. Fig. 10 shows the temporal waveform of a PPM-UWB signal. The electrical spectrum of the PPM-UWB signal is also shown. Due to the small DGD of PMF2, the time shift of the pulses for 0 and 1 bits is only $\sim$38 ps, making the pulse-position-modulated signal look like a Gaussian monocycle train. As a result, we cannot see any visible continuous part in the electrical spectrum, showing the modulation efficiency is

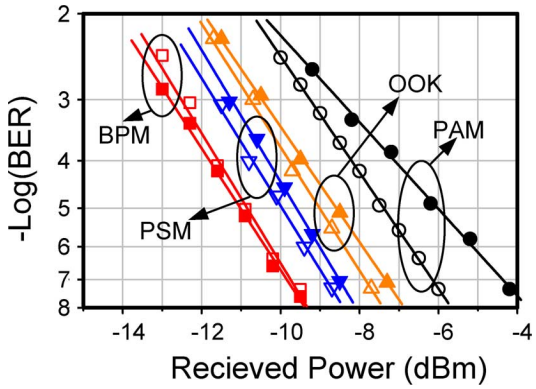

Fig. 9. BER measurements of the UWBoF system with OOK, BPM, PAM, and PSM. Hollow symbols: after wireless transmission. Solid symbols: after 20-km SMF and wireless transmission.

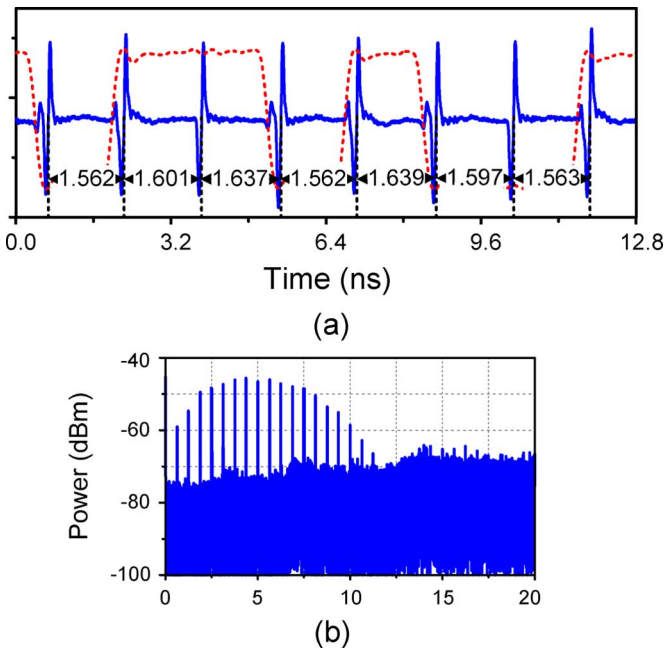

Fig. 10. Temporal waveform and the electrical spectrum of the UWB signal with PPM.

very low. Due to the low modulation efficiency, the BER performance cannot be evaluated. If a longer PMF with a larger DGD is used, higher modulation efficiency should be achieved.

It is worth noting that it is possible to integrate the AMZI and the $LiNbO_3$ PM in a monolithic chip [19]. In this case, the modulation schemes can be implemented by electrically switching the phase difference between the two arms in the AMZI. As a result, the system would be greatly simplified by the photonic integrated circuit technology, and the performance would be significantly improved. In addition, the generation of UWB signals in the optical domain would also simplify the entire system since no extra electrical to optical conversion is needed.

V. Conclusion

A comprehensive study on the implementation of multiple modulation schemes, i.e., OOK, BPM, PAM, PSM, and PPM, in an UWBoF system based on a PM and an electrical reconfigurable AMZI was performed. The impact of the fiber transmission on the PSD (or electrical spectra) of the UWB signals with OOK, BPM, PAM, and PSM schemes was theoretically studied and experimentally evaluated. An excellent agreement between the theoretical and the experimental results was achieved. For all the modulation schemes, the UWBoF system with 20-km SMF and wireless transmission could reach an error-free operation. The power penalties were less than 1.8 dB. Especially, for a BPM-based UWBoF system, a negative power penalty was achieved due to the positive impact of the fiber CD.

The system is potentially integratable, which may provide a simple and cost-effective solution for practical applications. In addition, the theory developed in this paper can be extended to study the modulation schemes implemented by other UWB signal generation systems.

References

[1] G. R. Aiello and G. D. Rogerson, "Ultra-wideband wireless systems," *IEEE Microw. Mag.*, vol. 4, no. 2, pp. 36–47, Jun. 2003.

[2] D. Porcino and W. Hirt, "Ultra-wideband radio technology: Potential and challenges ahead," *IEEE Commun. Mag.*, vol. 41, no. 7, pp. 66–74, Jul. 2003.

[3] M. Ghavami, L. B. Michael, and R. Kohno, *Ultra Wideband Signals and Systems in Communication Engineering*. West Sussex, U.K.: Wiley, 2004.

[4] I. Oppermann, M. Hämäläinen, and J. Iinatti, *UWB Theory and Applications*. Chichester, U.K.: Wiley, 2004.

[5] J. P. Yao, F. Zeng, and Q. Wang, "Photonic generation of ultrawideband signals," *J. Lightw. Technol.*, vol. 25, no. 11, pp. 3219–3235, Nov. 2007.

[6] C. M. Tan, L. C. Ong, M. L. Yee, B. Luo, and P. K. Tang, "Direct transmission of ultra wide band signals using single mode radio-over-fiber system," in *Proc. Asia-Pacific Microw. Conf.*, Suzhou, China, Dec. 2005, vol. 2, .

[7] C. S. Lim, M. L. Yee, and C. S. Ong, "Performance of transmission of ultra wideband signals using radio-over-fiber system," in *Proc. ITS Tele. Conf.*, Jun. 2006, pp. 250–253.

[8] M. L. Yee, L. C. Ong, C. K. Sim, B. Luo, and A. Alphones, "Low-cost radio-over-fiber in-building distribution network for WLAN, UWB and digital TV broadcasting," in *Proc. Asia-Pac. Microw. Conf.*, 2006, pp. 95–98.

[9] L. C. Ong, M. L. Yee, and B. Luo, "Transmission of ultra wideband signals through radio-over-fiber systems," in *Proc. IEEE Lasers Electr.-Opt. Soc.*, Oct. 2006, pp. 522–523.

[10] R. Llorente, T. Alves, M. Morant, M. Beltran, J. Perez, A. Cartaxo, and J. Marti, "Ultra-wideband radio signals distribution in FTTH networks," *IEEE Photon. Technol. Lett.*, vol. 20, no. 10, pp. 945–947, May 2008.

[11] M. P. Thakur, T. J. Quinlan, C. Bock, S. D. Walker, M. Toycan, S. E. M. Dudley, D. W. Smith, A. Borghesani, D. Moodie, M. Ran, and Y. Ben-Ezra, "480-Mbps, bi-directional, ultra-wideband radio-over-fiber transmission using a 1308/1564-nm reflective electro-absorption transducer and commercially available VCSELs," *J. Lightw. Technol.*, vol. 27, no. 3, pp. 266–272, Feb. 2009.

[12] Y. Le Guennec, A. Pizzinat, S. Meyer, B. Charbonnier, P. Lombard, M. Lourdiane, B. Cabon, C. Algani, A. L. Billabert, M. Terre, C. Rumelhard, J. L. Polleux, H. Jacquinot, S. Bories, and C. Sillans, "Low-cost transparent radio-over-fiber system for in-building distribution of UWB signals," *J. Lightw. Technol.*, vol. 27, no. 14, pp. 2649–2657, Jul. 15, 2009.

[13] T. B. Gibbon, X. B. Yu, D. Zibar, and I. T. Monroy, "Novel ultra-wideband photonic signal generation and transmission featuring digital signal processing bit error rate measurements," in *Proc. OFC/NFOEC*, 2009, pp. 1–3, Paper OTuB8.

[14] S. L. Pan and J. P. Yao, "Photonic generation and transmission of UWB signals with on-off keying and bi-phase modulation schemes," presented at the Optoelectron. Commun. Conf., Hong Kong, 2009, Paper TuH2.

[15] S. L. Pan and J. P. Yao, "Photonic generation of chirp-free UWB signals for UWB over fiber applications," presented at the IEEE Int. Topical Meeting Microw. Photon., Valencia, Spain, Oct. 14–16, 2009, Paper Th3.7.

[16] S. L. Pan and J. P. Yao, "Transmission of 1.25-Gb/s quasi-single-sideband Optical UWB signals over single-mode fiber," in *Proc. IEEE Radio Wireless Symp.*, 2010, pp. 500–503, Paper WE3C-2.
[17] M. Abtahi, M. Mirshafiei, S. LaRochelle, and L. A. Rusch, "All-optical 500-Mb/s UWB transceiver: An experimental demonstration," *J. Lightw. Technol.*, vol. 26, no. 15, pp. 2795–2802, Aug. 2008.
[18] C. Wang, F. Zeng, and J. P. Yao, "All-fiber ultrawideband pulse generation based on spectral-shaping and dispersion-induced frequency-to-time conversion," *IEEE Photon. Technol. Lett.*, vol. 19, no. 3, pp. 137–139, Feb. 2007.
[19] S. L. Pan and J. P. Yao, "Switchable UWB pulse generation using a phase modulator and a reconfigurable asymmetric Mach–Zehnder interferometer," *Opt. Lett.*, vol. 34, no. 2, pp. 160–162, Jan. 2009.
[20] F. Zeng and J. P. Yao, "Ultrawideband impulse radio signal generation using a high-speed electrooptic phase modulator and a fiber-Bragg-grating-based frequency discriminator," *IEEE Photon. Technol. Lett.*, vol. 18, no. 19, pp. 2062–2064, Oct. 2006.
[21] V. Torres-Company, K. Prince, and I. T. Monroy, "Fiber transmission and generation of ultrawideband pulses by direct current modulation of semiconductor lasers and chirp-to-intensity conversion," *Opt. Lett.*, vol. 33, no. 3, pp. 222–224, Feb. 2008.
[22] S. L. Pan and J. P. Yao, "An optical UWB pulse generator for flexible modulation format," *IEEE Photon. Technol. Lett.*, vol. 21, no. 19, pp. 1381–1383, Sep. 2009.
[23] J. J. Dong, X. L. Zhang, J. Xu, D. X. Huang, S. N. Fu, and P. Shum, "Ultrawideband monocycle generation using cross-phase modulation in a semiconductor optical amplifier," *Opt. Lett.*, vol. 32, no. 10, pp. 1223–1225, May 15, 2007.
[24] Q. Wang, F. Zeng, S. Blais, and J. P. Yao, "Optical ultrawideband monocycle pulse generation based on cross-gain modulation in a semiconductor optical amplifier," *Opt. Lett.*, vol. 31, no. 21, pp. 3083–3085, Nov. 2006.
[25] Q. Wang and J. P. Yao, "Switchable optical UWB monocycle and doublet generation using a reconfigurable photonic microwave delay-line filter," *Opt. Exp.*, vol. 15, no. 22, pp. 14667–14672, Oct. 2007.
[26] H. Chen, M. Chen, C. Qiu, J. Zhang, and S. Xie, "UWB monocycle pulse generation by optical polarisation time delay method," *Electron. Lett.*, vol. 43, no. 9, pp. 542–543, Apr. 2007.
[27] J. Q. Li, S. N. Fu, K. Xu, J. Wu, J. T. Lin, M. Tang, and P. Shum, "Photonic ultrawideband monocycle pulse generation using a single electro-optic modulator," *Opt. Lett.*, vol. 33, no. 3, pp. 288–290, Feb. 2008.
[28] J. Wang, Q. Z. Sun, J. Q. Sun, and W. W. Zhang, "All-optical UWB pulse generation using sum-frequency generation in a PPLN waveguide," *Opt. Exp.*, vol. 17, no. 5, pp. 3521–3530, Mar. 2009.
[29] G. H. Smith, D. Novak, and Z. Ahmed, "Overcome chromatic-dispersion effects in fiber wireless systems incorporating external modulators," *IEEE Trans. Microw. Theory Tech.*, vol. 45, no. 8, pp. 1410–1415, Aug. 1997.
[30] S. L. Pan and J. P. Yao, "A UWB over fiber transmitter reconfigurable for multiple modulation schemes," in *Proc. 35th Eur. Conf. Exhib. Opt. Commun. (ECOC)*, Vienna, Austria, Sep. 20–24, 2009, p. 2, Paper P6.04.
[31] S. L. Pan and J. P. Yao, "An analysis on the transmission of UWB signals over optical fiber," *IEEE J. Sel. Area Commun.*, vol. 28, no. 6, pp. 899–900, Aug. 2010.
[32] J. D. Bull, N. A. F. Jaeger, H. Kato, M. Fairburn, A. Reid, and P. Ghanipour, "40 GHz electro-optic polarization modulator for fiber optic communication systems," in *Proc. SPIE*, 2004, vol. 5577, pp. 133–143.
[33] C. D. Poole and R. E. Wagner, "Phenomenological approach to polarization dispersion in long single-mode fibers," *Electron. Lett.*, vol. 22, no. 19, pp. 1029–1030, Sep. 1986.
[34] G. P. Agrawal, *Nonlinear Fiber Optics*. San Diego, CA: Academic, 2001.
[35] U. Gliese, S. Norskov, and T. N. Nielsen, "Chromatic dispersion in fiber-optic microwave and millimeter-wave links," *IEEE Trans. Microw. Theory Tech.*, vol. 44, no. 10, pp. 1716–1724, Oct. 1996.

Shilong Pan (S'06–M'09) received the B.S. and Ph.D. degrees in electronics engineering from Tsinghua University, Beijing, China, in 2004 and 2008, respectively.

In August 2008, he joined the Microwave Photonics Research Laboratory, School of information Technology and Engineering, University of Ottawa, Ottawa, ON, Canada, as a Postdoctoral Research Fellow. His current research interests include fiber amplifiers and lasers, microwave photonics, optical signal processing, and terahertz wave generation.

Dr. Pan is a member of the Optical Society of America and the IEEE Photonics Society.

Jianping Yao (M'99–SM'01) received the Ph.D. degree in electrical engineering from the Université de Toulon, Toulon, France, in 1997.

In 2001, he joined the School of Information Technology and Engineering, University of Ottawa, Ottawa, ON, Canada, where he is currently a Professor, the Director of the Microwave Photonics Research Laboratory, and the Director of the Ottawa-Carleton Institute for Electrical and Computer Engineering. From 1999 to 2001, he was a Faculty Member at the School of Electrical and Electronic Engineering, Nanyang Technological University, Singapore. He is a Yongqian Endowed Visiting Chair Professor at Zhejiang University, China. He spent three months as an Invited Professor in the Institut National Polytechnique de Grenoble, France, in 2005. He is the author or coauthor of more than 280 papers, including more than 160 papers in refereed journals, and more than 120 papers in conference proceeding. He is an Associate Editor of the *International Journal of Microwave and Optical Technology*. His research interests include microwave photonics, including all-optical microwave signal processing, photonic generation of microwave, millimeter-wave, and THz, radio over fiber, ultra wideband over fiber, fiber Bragg gratings for microwave photonics applications, and optically controlled phased array antenna. Other research interests include fiber lasers, fiber-optic sensors, and biophotonics.

Prof. Yao is a Fellow of the Optical Society of America, and a Senior Member of the IEEE Photonics Society and the IEEE Microwave Theory and Techniques Society, and a Registered Professional Engineer of Ontario. He is on the Editorial Board of the IEEE TRANSACTIONS ON MICROWAVE THEORY AND TECHNIQUES. He was named the University Research Chair in Microwave Photonics in 2007. He was the recipient of the 2005 International Creative Research Award of the University of Ottawa, the 2007 George S. Glinski Award for Excellence in Research, and the Natural Sciences and Engineering Research Council of Canada Discovery Accelerator Supplements Award in 2008.